AGU PUBLICATIONS

Geochemistry, Geophysics, Geosystems

RESEARCH ARTICLE
10.1002/2015GC005797

Special Section:
Oceanic Detachment Faults

Tectonic evolution of 200 km of Mid-Atlantic Ridge over 10 million years: Interplay of volcanism and faulting

Johnson R. Cann[1], Deborah K. Smith[2], Javier Escartin[3], and Hans Schouten[2]

[1]School of Earth and Environment, University of Leeds and Curlew Cottage, Penrith, UK, [2]Department of Geology and Geophysics, Woods Hole Oceanographic Institution, Woods Hole, Massachusetts, USA, [3]Institut de Physique du Globe de Paris, CNRS UMR 7154 1, Paris, France

Key Points:
- 10 Ma tectonic history of spreading along 200 km of the Mid-Atlantic Ridge
- At any one time 70% of the axis has detachment faulting on one or both sides
- Relationship between detachment faulting and axial magmatism is not strong

Correspondence to:
J. Cann,
J.R.Cann@leeds.ac.uk

Citation:
Cann, J. R., D. K. Smith, J. Escartin, and H. Schouten (2015), Tectonic evolution of 200 km of Mid-Atlantic Ridge over 10 million years: Interplay of volcanism and faulting, *Geochem. Geophys. Geosyst.*, *16*, 2303–2321, doi:10.1002/2015GC005797.

Received 26 FEB 2015
Accepted 2 JUN 2015
Accepted article online 5 JUN 2015
Published online 22 JUL 2015

Abstract We reconstruct the history of the mode of accretion of an area of the Mid-Atlantic Ridge south of the Kane fracture zone using bathymetric morphology. The area includes 200 km of the spreading axis and reaches to 10 Ma on either side. We distinguish three tectonic styles: (1) volcanic construction with eruption and intrusion of magma coupled with minor faulting, (2) extended terrain with abundant large-offset faults, (3) detachment faulting marked by extension on single long-lived faults. Over 40% of the seafloor is made of extended terrain and detachment faults. The area includes products of seven spreading segments. The spreading axis has had detachment faulting or extended terrain on one or both sides for 70% of the last 10 Ma. In some parts of the area, regions of detachment faulting and extended terrain lie close to segment boundaries. Regions of detachment faulting initiated at 10 Ma close to the adjacent fracture zones to the north and south, and then expanded away from them. We discuss the complex evidence from gravity, seismic surveys, and bathymetry for the role of magma supply in generating tectonic style. Overall, we conclude that input of magma at the spreading axis has a general control on the development of detachment faulting, but the relationship is not strong. Other factors may include a positive feedback that stabilizes detachment faulting at the expense of volcanic extension, perhaps through the lubrication of active detachment faults by the formation of low friction materials (talc, serpentine) on detachment fault surfaces.

1. Introduction

At slow spreading ridges such as the Mid-Atlantic Ridge (MAR), the oceanic lithosphere is recognized as forming by two distinct modes of spreading, the volcanic mode and the detachment mode. In the volcanic mode, most of the extension takes place by magmatic processes such as injection of dykes and eruption of lavas, with a minor contribution from faulting. In the detachment mode, a large part of the extension takes place on large-offset normal faults with a less important and variable volcanic contribution [e.g., *Tucholke et al.*, 2008], coupled with the exposure of plutonic rocks [e.g., *Karson*, 1999; *Tucholke et al.*, 1998] and with high rates of hydroacoustic seismicity [*Escartín et al.*, 2008]. The detachment mode generates a distinctive range of bathymetric morphologies very different from the equally distinctive morphologies that characterize the volcanic mode [*Cannat et al.*, 2006; *Okino et al.*, 2004; *Smith et al.*, 2006, 2008, 2014; *Tucholke et al.*, 1998].

Using the distinctive bathymetric morphologies and the patterns of hydroacoustically recorded seismicity, *Escartín et al.* [2008] deduced the distribution of active detachment faulting along the slow spreading axis of the MAR between 12°N and 35°N and concluded that about half of the 2500 km of the ridge was spreading by detachment faulting on one flank or other and the other half of the ridge was volcanic on both sides. *Escartín et al.* [2008] did not identify any examples where the detachment mode is present on both sides of the axis. Other studies have shown instances where both sides of the axis are in the detachment mode such as at 15°N in the MAR [*Schroeder et al.*, 2007] and along a major section of the ultraslow spreading Southwest Indian Ocean Ridge [*Cannat et al.*, 2006; *Sauter et al.*, 2013], where extension along low-angle faults results in large, widely spaced smooth ridges that lack corrugations. In these instances the detachment faults appear to alternate from one side to the other of a broad axial zone, with no well-defined median valley.

In this paper, we use the distinctive morphologies of the two modes of spreading to develop a new tectonic interpretation of a region of the MAR between 22°N and 24°N, south of the Kane fracture zone. We build on

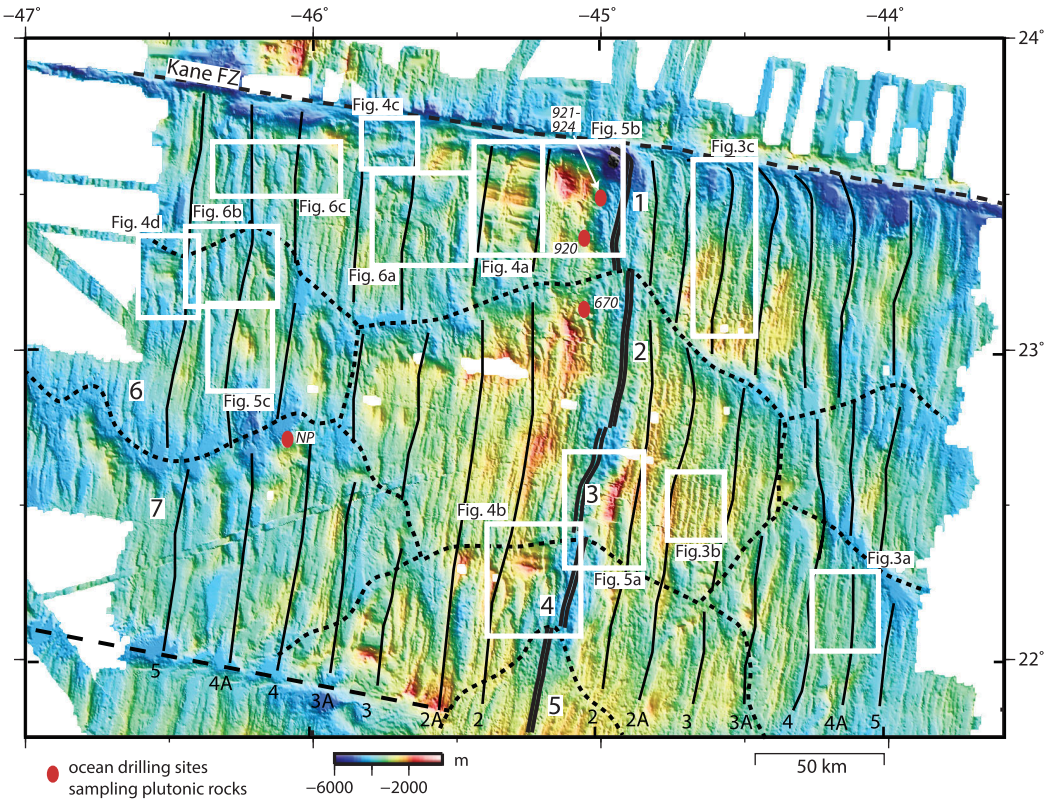

Figure 1. Bathymetric map of the study area. The Kane fracture zone borders the area on the north and an unnamed fracture zone lies close to the southern edge. The spreading axis is marked by a double black line. Large black numbers along the axis identify the spreading segments recognized in this paper (1–5 from north to south). Long black dashed lines: transform faults. Short black dashed lines: off-axis boundaries of the regions corresponding to the axial segments. Off-axis the areas for Segments 2 and 3 are united. Areas generated at extinct spreading segments are numbered 6 and 7. Magnetic anomalies derived from *Gente et al.* [1995] are labeled with small black numbers. White boxes: areas enlarged in Figures 2–5. White letters KMM identify the Kane Megamullion, the area described in detail in *Dick et al.* [2008]. Red ovals: ocean drilling sites labeled with hole numbers or with NP standing for North Pond.

existing work in the area [e.g., *Cannat et al.*, 1995b; *Gente et al.*, 1995, and other references below]. Our study area (Figure 1) extends for ∼200 km along the axis and for 120 km on either side of the axis, equivalent to 10 Ma of spreading. On the north it is bordered by the Kane fracture zone, with a sinistral offset of about 100 km. To the south the border was another fracture zone with about 40 km of dextral offset until about 3 Ma ago, when a volcanically active segment propagated northward across the fracture zone.

The size of the area allows us to examine the relationship between the different modes of spreading and to investigate the possible controls on the transition from one mode to another both along and across the spreading axis. We use the bathymetric signals to map the distribution of the different modes across the area as a function of time and space. We examine the nature of the boundaries between lithosphere constructed by the different accretion modes. We reconstruct the nature of the spreading axis as a function of time and are able to set constraints on the development of the accretion modes and their evolution.

2. The Study Region and Existing Data

The South of Kane area (Figure 1) has been the site of several studies many of which provide crucial ground-truth for this investigation and include seafloor observations. These range from early geological work [e.g., *Bryan et al.*, 1981; *Karson and Dick*, 1983; *Melson et al.*, 1968; *Miyashiro et al.*, 1971] that is complemented by later studies including geophysical and seismological surveys [e.g., *Canales et al.*, 2000; *Cannat et al.*, 1995b; *Gente et al.*, 1995; *Maia and Gente*, 1998; *Pockalny et al.*, 1995; *Purdy and Detrick*, 1986]. More recent detailed work of *Dick et al.* [2008] describes both the geology and geophysics of the Kane Megamullion region adjacent to the Kane transform and the conjugate to it on the east side of the axis. Many of these investigations recovered plutonic rocks by dredging or submersible indicating the presence of detachment faulting. Several of the

ocean drilling legs in the study region reached plutonic rock. DSDP Leg 45 drilled at Site 395 in the North Pond basin (labeled NP in Figure 1) and penetrated a sedimentary unit of plutonic rocks, including gabbro and serpentinite, sandwiched between basaltic lava flows [*Melson et al*., 1979]. This deep hole was the subject of downhole logging experiments on several later DSDP and ODP legs [e.g., *Becker et al*., 1984]. More recently IODP Leg 336 drilled at Site 1382 close to Site 395 in North Pond and deployed a subseafloor observatory [*Edwards et al*., 2012]. Hole 1382A penetrated a sedimentary unit containing plutonic rocks very similar to that in Hole 395A. ODP Legs 109 (Site 670) and 153 (Sites 920–924) (Figure 1) penetrated plutonic rock near the axis and close to the Kane transform [*Andreani et al*., 2007; *Cannat et al*., 1995a; *Detrick et al*., 1990]. A wide-angle seismic profile [*Canales et al*., 2000] over Site 920 and extending along a flow line on either side of the axis indicates that the crust in this region is very thin (<3 km) beneath both flanks of the median valley and also shows important variations in thickness along the profile. A seismic study of a massif at 22.3°N [*Dannowski et al*., 2010] showed the presence of thin (~4 km) crust beneath the massif, interpreted as a detachment fault core complex, compared with normal crustal thickness (~6 km) beneath the valley floor and the eastern side of the axis.

Our analysis of the modes of spreading was made with multibeam bathymetry data obtained from the Global Multiresolution Topography Data Portal (http://www.marine-geo.org/portals/gmrt/), and first reported by *Gente et al*. [1995] and *Cannat et al*. [1995b]. To examine these modes closely enough, the bathymetry data were gridded at 100 m, contoured at a 25 m interval and assessed at a scale of 1:250,000 (Figure 1). Critical to our interpretation was a very close examination of the bathymetric features, kilometer by kilometer throughout the area, as described in *Smith et al*. [2008]. To constrain the spreading history of the area, we used the magnetic anomaly identifications of *Gente et al*. [1995], which are shown in Figure 1. *Williams* [2007] also identified magnetic anomalies in this area using data collected more recently. These identifications are very close to those of *Gente et al*. [1995] but do not cover the whole of the study area, so for consistency we retain the earlier interpretations.

As is often the case in the Atlantic, the anomalies are not everywhere precisely defined. The area contains anomalies from 1 to 5 on each side corresponding to 10 Ma of spreading at a total rate of 25 mm/yr. In the north of the area the spreading has been very asymmetric, about 1.4 times faster on the west than on the east for the whole period. In the south the spreading has been nearly symmetric overall. The transition from the northern asymmetric spreading to the southern symmetric spreading takes place rather rapidly about half way along the axis in the area.

Based on evidence from bathymetry and gravity, *Gente et al*. [1995] mapped a tessellated pattern of the crust away from the spreading axis. This was interpreted as representing the evolution of segmentation through time, as magmatic segments have grown and shrunk. Gente et al.'s pattern is a very complex one and has two significant weaknesses:

1. It does not take full account of the morphology of the volcanic ridges on either side of the axis, though these must be the primary indicators of original offsets of the spreading axis.
2. It is not approximately symmetrical about the axis, governed by the magnetic anomalies, which is necessary if it represents past offsets of the axis. We have reassessed this interpretation and developed an alternative, simpler version for use in this paper. This is discussed below in section 4.2.

3. Identifying Modes of Spreading

In this section we develop the relation between the tectonic variety of the MAR and the related morphological features and shown schematically in Figure 2, illustrating the discussion with examples from the study area, developing the discussion further than has been done previously [*Smith et al*., 2006; 2008]. Here we use the term "outward-facing" to mean facing away from the spreading axis. Similarly "inward-facing" means facing toward the spreading axis.

3.1. Volcanic Morphology of the Spreading Axis

In most spreading segments of the northern MAR, independent of the spreading mode of the flanks of the ridge, an axial volcanic ridge (AVR) runs along the middle of the median valley floor. AVRs are typically several tens of kilometers long, and are shallowest toward their center, deepening toward their ends. These

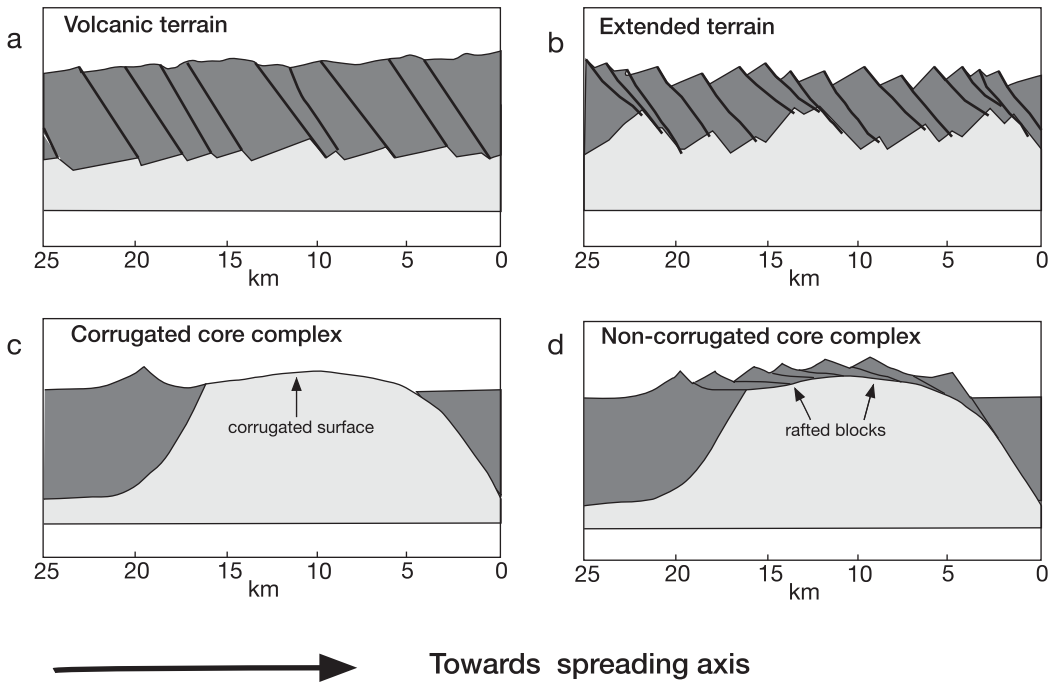

Figure 2. Schematic cross sections through the four different styles of accretion described in this paper. (a) Accretion dominated by volcanics with minor faulting. (b) Extension of the volcanics at a higher degree of faulting. (c) Corrugated core complex with a very large offset fault exposing the fault plane and the footwall basement below it. (d) Noncorrugated core complex with the fault plane concealed below overlapping rafted blocks.

volcanic ridges are typically 200–400 m high and 3–4 km wide, so that the flanks of the AVRs dip away from the crest of the ridges at $<\sim 10^{\circ}$. The bathymetry shows a range of volcanic features on the flanks of AVRs. These include small volcanic cones, some with flat tops or craters, lava flow ridges and terraces, and more substantial volcanic edifices [*Searle et al*., 2010; *Smith and Cann*, 1999]. The flat tops of volcanic cones are close to horizontal, probably reflecting ponded lava flow lobes. In some places, smooth, flat areas represent more extensive flows that fill the topography. This morphology can only be seen in a detailed examination of the bathymetry. Identification of this range of features as produced by basaltic volcanism has been confirmed repeatedly by dredging and submersible observation since the first multibeam maps were made of mid-ocean ridges [*Ballard and van Andel*, 1977].

3.2. Volcanic Mode of Spreading

In the volcanic mode of spreading, toward the edge of the median valley floor the volcanic morphology is cut by steep inward-facing faults. Slices of the AVR, typically 5–10 km wide, are transported upward and out of the median valley. Off-axis, areas of volcanically constructed seafloor can be recognized by parallel elongate abyssal hill ridges, each typically several tens of kilometers long, spaced 5–10 km apart and running parallel to the spreading axis. These have a quite distinct morphology from the much higher relief and shorter ridges that mark extensive exposures of peridotite forming part of the "smooth seafloor" system [*Cannat et al*., 2006] that lack any sign of volcanic morphology. The abyssal hill ridges are bordered by gentle (typically $<\sim 10^{\circ}$) slopes on the outward-facing side. On close examination of the bathymetry these outward-facing slopes show the same range of volcanic features as are seen on the flanks of the AVRs. The flat tops of small volcanoes or ponded flow lobes are close to horizontal, suggesting very limited seafloor rotation since the volcanic construction ended. Examples from the study area are shown in Figure 3. Field observations confirming our interpretation come from submersible dives within the area of Figure 3c along a line from 44°40′W to 44°35′W at latitude 23°20′N [*Durand et al*., 1996]. We interpret the abyssal hill ridges, as many others have done before [e.g., *Kong et al*., 1988; *Pockalny et al*., 1988; *Sempéré et al*., 1993; *Shaw and Lin*, 1993], as strips of the volcanic seafloor of the median valley floor cutoff by steep normal faults throwing down toward the spreading axis. These faults have similar morphology to the faults that border the median valley. Groups of abyssal hill ridges commonly terminate at discontinuities corresponding to original offsets in the spreading axis within the median valley. As abyssal hill ridges approach a

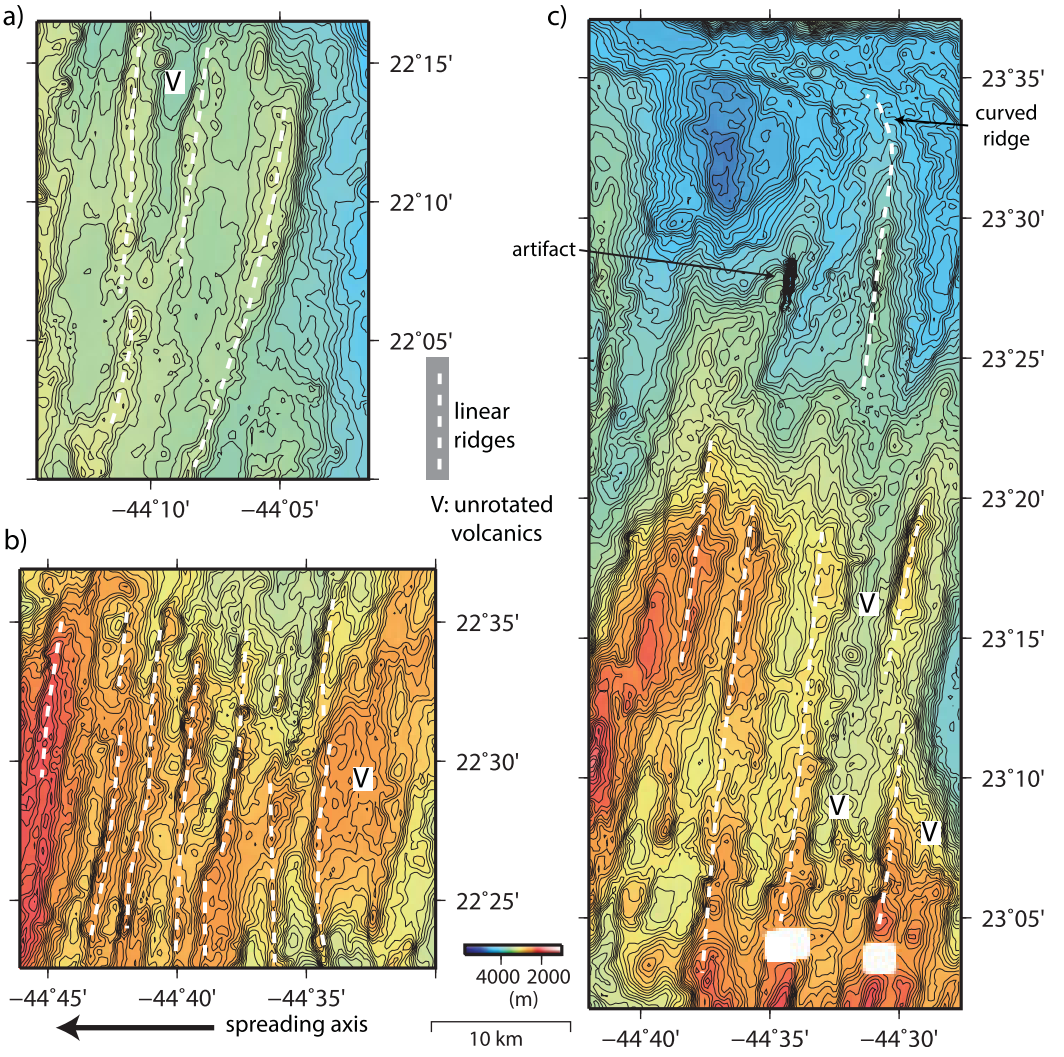

Figure 3. Examples of volcanic bathymetric morphology, contoured at 50 m intervals. Locations are shown in Figure 1. The spreading axis lies to the west in each image. The map of the whole study area was examined at the same resolution and with the same contour interval as in this image. White dashed lines are abyssal volcanic ridges. Note the steep sides to the ridges on the inward-facing sides toward the spreading axis, interpreted as marking small-offset faults throwing down toward the axis. Note the small volcanic features on the gently dipping outward-facing sides of the ridges, including small flat-topped flow features and small volcanic hummocks. V marks areas of unrotated volcanics. Figure 3c is at the north end of the area on the east side of the spreading axis. Note the hooking of the abyssal volcanic ridges as they approach the Kane fracture zone, curving in the same direction as the offset of the transform fault.

discontinuity, over the last few kilometers they typically hook toward the discontinuity, especially if the abyssal hill ridge formed on the outside corner of the offset. A schematic section through such terrain is shown in Figure 2a.

3.3. Detachment Mode of Spreading

In the detachment mode, the steep normal faults that border the median valley continue to extend until the slip on the fault reaches or exceeds several kilometers. During such a large slip, the footwalls of the faults rotate outward, flattening the fault planes and tilting the originally near-horizontal volcanic seafloor on the outward side of the fault breakaway by up to several tens of degrees [*Garces and Gee*, 2007; *MacLeod et al*., 2011; *Morris et al*., 2009; *Smith et al*., 2008; *Tucholke et al*., 1998]. The resulting topography has typically greater relief and a shorter length scale parallel to the spreading axis than that of the volcanic mode, indicating that originally long fault systems become partitioned into shorter sections as extension increases. As the extension develops there are two different outcomes, formation of a core complex and formation of consecutive large-offset faults.

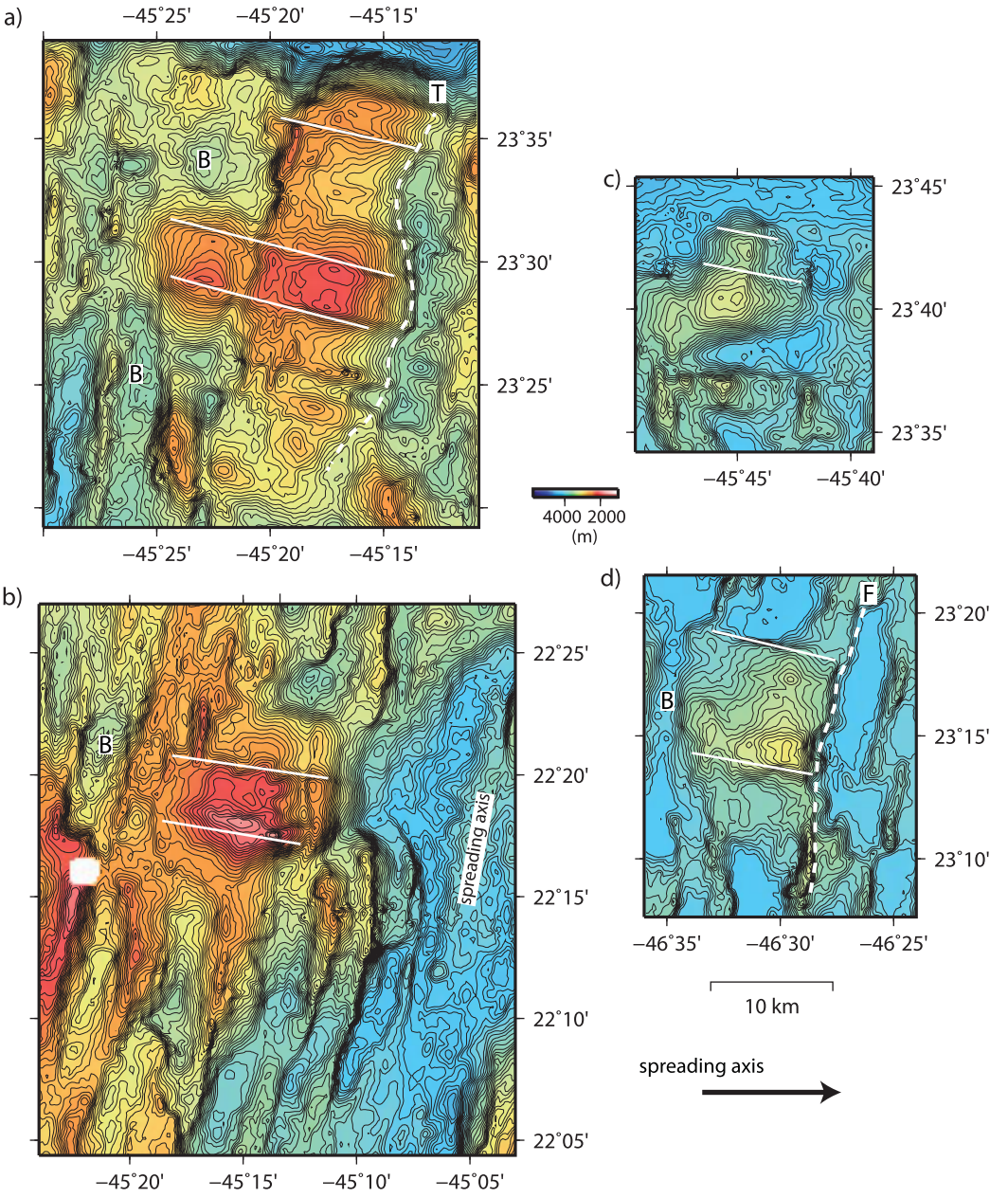

Figure 4. Examples of corrugated core complexes. Bathymetry data are contoured at 50 m intervals, and locations are shown in Figure 1. In each map the spreading axis lies to the east. Examples of corrugations are marked by continuous white lines. T and associated dashed white line: the termination of the detachment (where termination refers to the line of emergence of the fault from the ocean floor). F and associated dashed white line: a later fault that has cut across the detachment fault. B marks small basins (see text for details). (a) The Kane Megamullion area described by *Dick et al.* [2008]. (b) Area described by *Dannowski et al.* [2010]. South of the core complex is a group of small faults emerging from the median valley floor. (c, d) Sites some way off-axis. (d) A good termination fault.

3.3.1. Core Complexes

In this area we distinguish two end-member types of core complex, corrugated core complexes, and non-corrugated core complexes (see examples of both end-members in our study area in Figures 4 and 5). Corrugated core complexes arise where the fault plane bordering the median valley continues to extend, rotating by flexure, until it forms the cap to a domal corrugated massif, the top of which may be close to horizontal (Figure 4). These massifs are typically 15–30 km in size parallel to the spreading axis, and a similar dimension perpendicular to the spreading axis, though a series of domes may be linked together continuously away from the axis for up to 100 km [*Ohara et al.*, 2001]. The corrugations run in the direction of spreading and have a wavelength of about 1 km when seen on the multibeam bathymetry data. They run

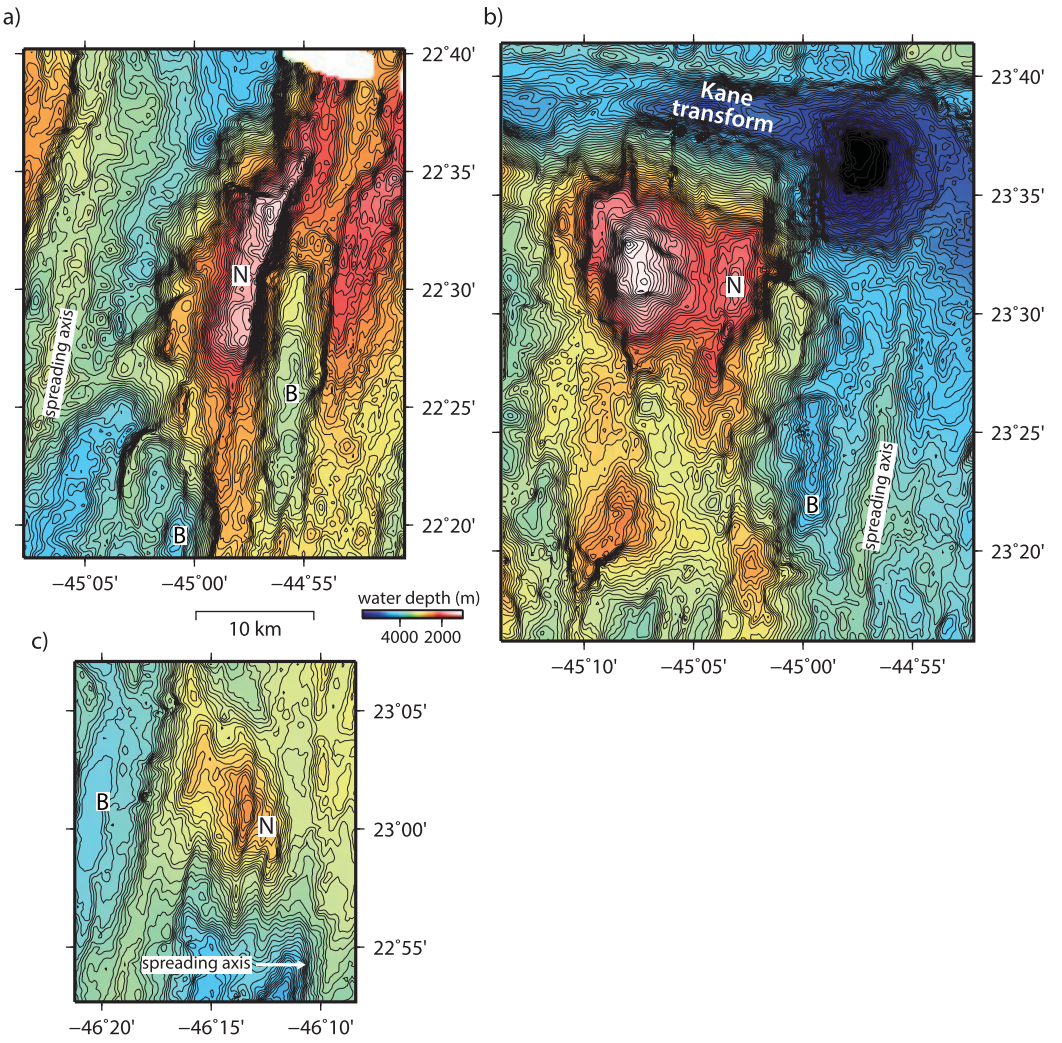

Figure 5. Examples of noncorrugated core complexes (labeled N). Bathymetry data are contoured at 50 m intervals, and locations are shown in Figure 1. (a) Active core complex on the east side of Segment 3. Note the steep outward-facing slope at its outward side and the rugged inward-facing side with small ridges parallel to the spreading axis. (b) Massif at the inside corner of the Kane transform fault; noncorrugated at its east end close to the spreading axis and corrugated at its west end. (c) Extinct noncorrugated massif west of the spreading axis. This has a steep breakaway showing rotated volcanic features and well-developed ridges parallel to the spreading axis. B: small oval basins common on the outward side of core complexes.

continuously over the top of the massif. On a more detailed scale, side-scan sonar images and bottom photographs show striations that run parallel to the corrugations [e.g., *Blackman et al.*, 2002; *MacLeod et al.*, 2002, 2009; *Mallows and Searle*, 2012]. Plutonic rocks (gabbro and ultramafic) are commonly recovered from the corrugated surfaces [*Cannat et al.*, 1995b; *Dick et al.*, 2008; *MacLeod et al.*, 2002]. Because of the flexural rotation of the fault as it slips, the breakaway of a core complex is commonly a ridge with an outward-facing slope greater than 15–20°. This slope shows volcanic morphology similar to that of one flank of an AVR, but tilted through tens of degrees [*Smith et al.*, 2008]. The slope is interpreted as the result of tilting of the median valley floor that capped the original fault block. Adjacent to the ridge on its outward-facing side is commonly a small oval basin elongate parallel to the spreading axis, 10–20 km long, apparently the result of footwall flexure that accompanied the extension and rotation of the fault (examples from the study area are shown in Figures 4 and 5). Major steep faults may cut core complexes, throwing down either toward or away from the spreading axis. A schematic cross section through a corrugated core complex is shown in Figure 2c.

Noncorrugated core complexes are massifs similar in size to the corrugated core complexes, but without corrugations. Instead in this area they are capped by ridges running parallel to the spreading axis. Noncorrugated core complexes in other parts of the MAR include the TAG massif at 26°N that is associated with a

steeply dipping zone of earthquakes, apparently following the detachment fault surface [*deMartin et al*., 2007], and the Logatchev massif at 15°N [*Grevemeyer et al*., 2013]. Figure 5 shows examples from the study area, including the massif close to the axis at 22°30′N. That is where an early ocean bottom seismometer deployment detected abundant microearthquakes down to 6 km depth [*Toomey et al*., 1988] and a later autonomous hydrophone array [*Smith et al*., 2003] recorded one of the highest rates of seismicity along the northern MAR. The high rates of seismicity and similar morphology suggest strong parallels with the TAG massif [*Smith et al*., 2003]. In places, between the ridges that cap the noncorrugated complexes, small strips of corrugated surface may be exposed. Dredge hauls from two of the noncorrugated massifs in the survey area recovered basalts, both fresh and metamorphosed [*Gillis and Thompson*, 1993; *Melson et al*., 1968]. We interpret such core complexes as massifs in which the detachment fault plane is partly or totally covered with rafted blocks [*Buck*, 1988; *Reston and Ranero*, 2011]. The ridges would correspond to the top edges of the faults that bound the rafted blocks. Oval basins and steep outward slopes similar to those on the outward side of corrugated core complexes are commonly also found associated with noncorrugated core complexes. A schematic section through a noncorrugated core complex covered by rafted blocks is shown in Figure 2d. Note the steep outward slopes generated by flexure of the rafted blocks.

Intermediate cases exist that combine features of both corrugated and noncorrugated core complexes, side by side. In places the corrugated surface lies on the inward-facing side, indicating an evolution from a noncorrugated core complex to a corrugated core complex as extension continues. Other cases show the reverse sense of evolution, with a corrugated surface facing outward away from the spreading axis and a noncorrugated section on the inward-facing side, as in the core complex at the current Kane inside corner (Figure 5b).

3.4. Extended Terrain

Some areas of the seafloor contain abundant narrow ridges with outward-facing slopes of $>25°$ and associated oval basins lying on the outward-facing sides of the ridges (Figure 6). The inward-facing slopes of these ridges are often irregular along their strike. We interpret such areas as representing a third style of accretion, intermediate between detachment faulting and volcanic construction. This style is generated by repeated large-offset faulting (offsets >3 km), producing an extended terrain. Individual core complex massifs may be set within such areas. The ridges have the same dimensions as those associated with the breakaways of core complexes (15–25 km long parallel to the axis). The associated basins are also similar in shape to those linked to core complexes (10–20 km long, about 5 km wide). We interpret the ridges in these regions as marking the tops of individual faults. There are two interpretations possible of such extended terrain. One is that consecutive large-offset faults form, each with a minimum of 3 km offset as suggested by modeling [*Schouten et al*., 2010; *Smith et al*., 2008], but that none of the faults extended far enough (8–10 km offset) to develop into a major detachment fault. The other is that these faults mark rafted blocks bounded by large-offset faults generated one by one at the spreading axis, all soling down into a continuous detachment fault at depth [*Buck*, 1988; *Reston and Ranero*, 2011]. At present we cannot distinguish between the two cases, but both would require a major extension of the seafloor by faulting. It is likely that the mean magnitude of flexural rotation would be different in the two cases, but this needs further investigation. A schematic cross section through an area of one kind of extended terrain is shown in Figure 2b. Note that the greater extension on the faults produces steep outward slopes associated with flexural basins.

3.5. Features Diagnostic of the Mode of Spreading

Four different types of features were mapped for the analysis, based on the description of the spreading modes above.

1. Abyssal hill ridges identified based on the length of the ridges (typically tens of kilometers), the characteristic morphology of lava flows and small seamounts on their outward-facing sides, the presence of steep inward-facing faults on their inward sides, and by the increasing depth and curvature of the crests of the ridges toward their ends (Figure 3).
2. Core complexes identified as positive bathymetric features showing the range of morphologies described above (Figures 4 and 5).
3. Ridges with outward slopes $>25°$, typically with shorter lengths than the abyssal hill ridges, and commonly with tilted volcanic features on their outward-facing sides.
4. Small oval basins, corresponding to flexural depressions, identified by their size and shape.

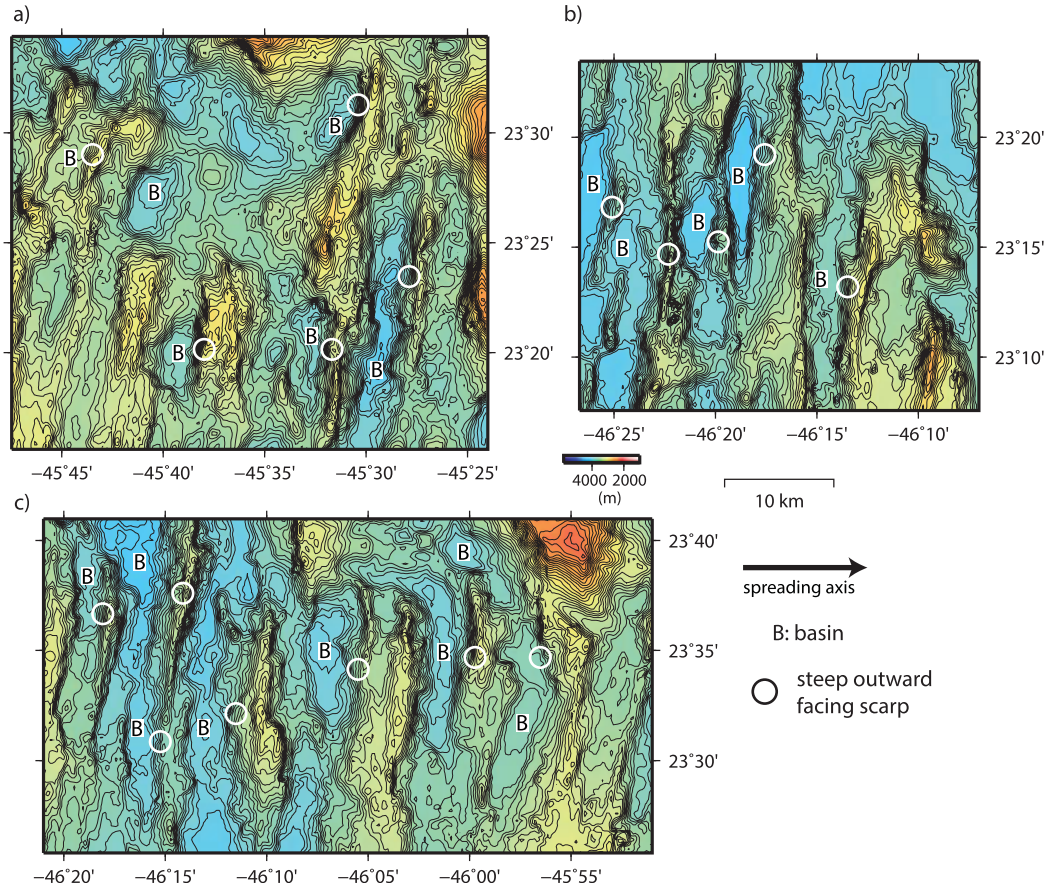

Figure 6. Examples of areas of extended terrain. (a–c) Bathymetry data contoured at 50 m intervals; locations are shown in Figure 1. In all three maps the spreading axis lies to the east (right). O: examples of outward-facing scarps dipping at greater than 25°. B: examples of small oval basins that are associated with the steep outward-facing scarps. To avoid concealing too many features, not all basins and steep outward-facing slopes are labeled.

These features are plotted in Figure 7, together with sites of recovery of plutonic rocks taken from *Cannat et al*. [1995b] and *Dick et al*. [2008].

4. Results

We consider first the nature of the current spreading axis, then the application of the bathymetric indicators to the area as a whole before considering the evolution of the spreading axis through time.

4.1. The Spreading Axis

We divide the median valley in the study area into five active segments, each laterally offset by a few kilometers from the next (Figures 1 and 7). The segment lengths and offsets shown are similar to those used in earlier work [e.g., *Maia and Gente*, 1998; *Thibaud et al*., 1998] though we divide their central Segment 2 into two, our Segments 2 and 3. The axis of each segment is marked by volcanic features such as a chain of small seamounts or an AVR. The northernmost segment (Segment 1, Figure 1) starts within the nodal basin at the Kane transform at 23°38′N, 44°53′W. Its axis is a well-developed AVR with fresh, glassy lavas, the Snake Pit Ridge, host to the Snake Pit hydrothermal system [*Brown and Karson*, 1988; *Karson and Brown*, 1988] and the site of axial drilling during ODP Leg 106 [*Detrick et al*., 1990]. The section of the axis at 23°20′N is underlain by crust with low seismic velocities, and interpreted as indicating the presence of melt [*Canales et al*., 2000]. At 23°15′N there is an offset of ∼8 km to the east, at the start of Segment 2. The volcanic axis in Segment 2 contains an irregular AVR [*Kong et al*., 1988] that reaches its shallowest depth at 22°55′N and ends in a deep at 22°45′N, 44°58′W. The offset between Segments 2 and 3 is 4 km to the west. The volcanic axis

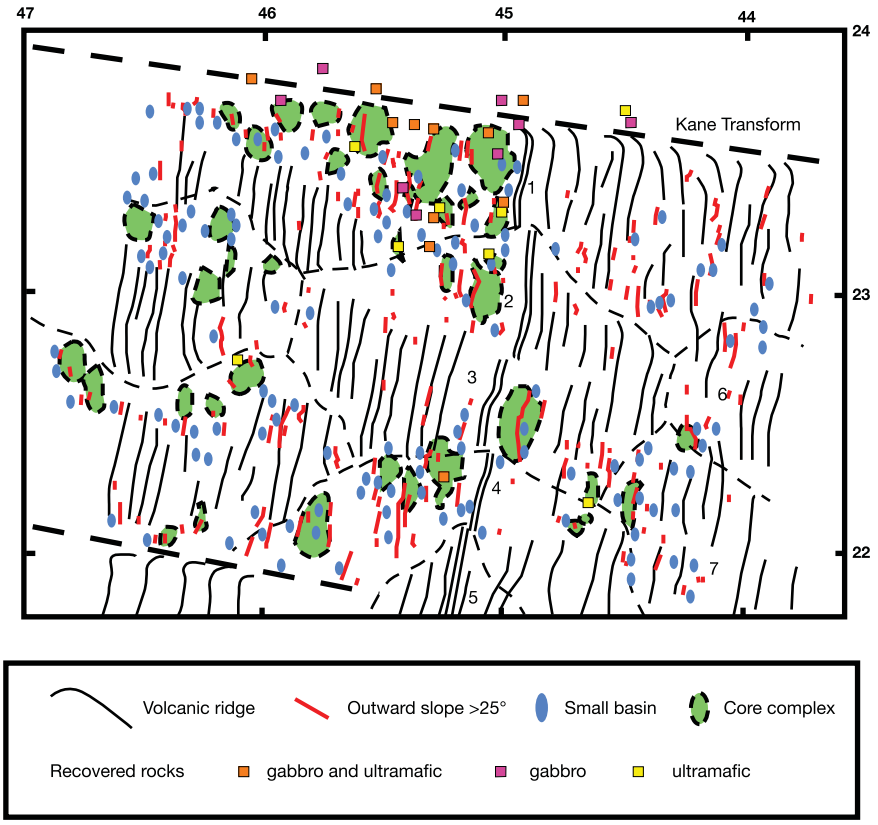

Figure 7. Distribution of morphological features with tectonic significance (see key to the figure). Note the association of steep outward-facing scarps, small basins, exposed core complexes, and plutonic rock samples. Some areas contain abundant exposed core complexes associated with the other indicators, while in other areas steep outward-facing scarps and small basins are abundant without the presence of exposed core complexes. The volcanic ridges are abundant in areas in which the other tectonic indicators are absent. Double black line: spreading axis.

in Segment 3 is displaced to the west side of the median valley. Segment 3 ends at 22°23′N and is succeeded by Segment 4, a short segment that ends at 22°10′N. Segment 4 contains a low-relief axial volcanic ridge. South of Segment 4 is the northern end of the active volcanic Segment 5 that extends beyond our study area as far south as 21°22′N.

The current spreading mode of each segment can be evaluated using the method of *Escartín et al*. [2008] who identified areas of active detachment faulting along a much greater length (∼2500 km) of the northern MAR ridge axis. Segment 1 shows evidence of detachment faulting all along the western side of the median valley from north to south, with a noncorrugated core complex at the northern end, then a ridge-basin pair and finally another core complex at its southern end (Figure 7). The eastern side of the median valley is volcanic along its length. Segment 2 shows volcanic morphology along its eastern side, and the morphology of detachment faulting along the western side of the median valley. Within the median valley a slice of the western side of the floor of the median valley has been cutoff by a newly formed axial valley wall fault, raising it above the AVR. This morphology indicates either that detachment faulting may have recently become inactive on the western side of the median valley, or that this slice of the median valley floor is an emerging rafted block that will eventually be rotated and join the detachment mode. In Segment 3 there is a noncorrugated core complex on the eastern side and extended terrain on the western side. There is a short length of the axis, at the south end of Segment 3 and the north end of Segment 4 where two core complexes face each other across the median valley floor. Segment 4 is very short, and has a conspicuous corrugated core complex on its western side and volcanic topography on the east. The north end of Segment 4 overlaps in part with the south end of Segment 3, indicating that two detachment terrains face each other across the spreading axis for a short distance. The southernmost segment (Segment 5) is volcanic on both sides, with very little evidence of extension by faulting.

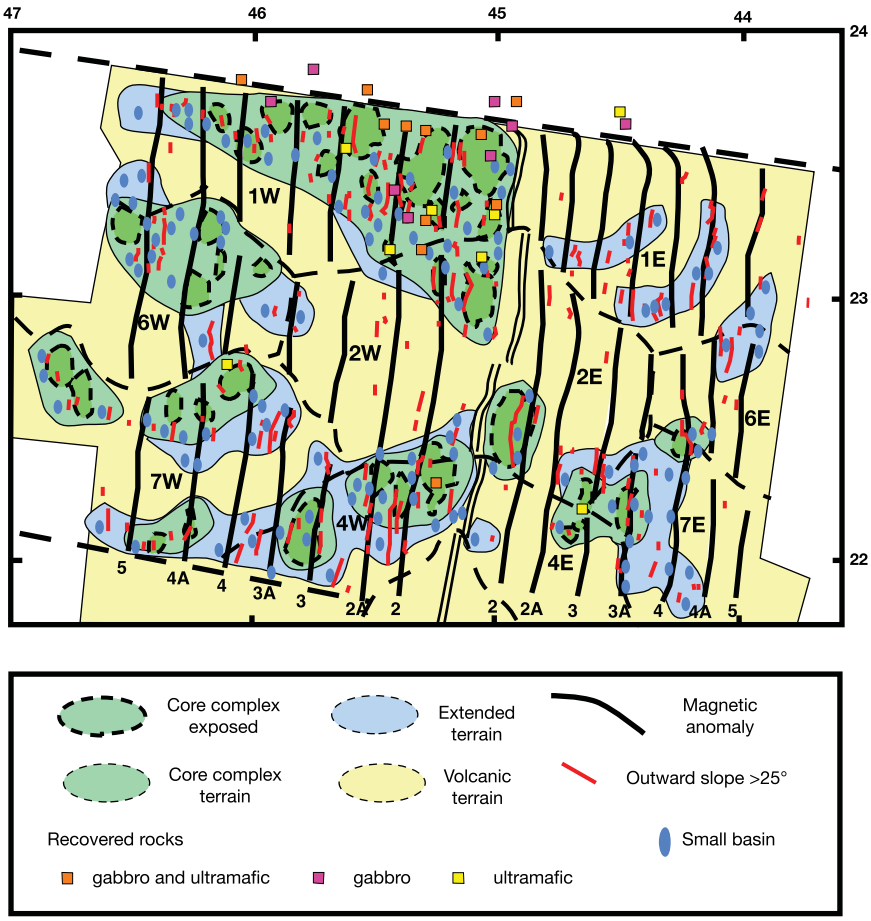

Figure 8. Generalization of the observations of Figure 7 to yield a tectonic interpretation of the survey area into three types of terrain—volcanic (V), core complex (C), and extended (E) terrains. The segment numbers are the same as in Figures 1 and 7. The areas generated at the different segments are labeled 1W (1 west), 1E, and so on. Note that off-axis no distinction is made between areas generated at Segments 2 and 3. The identification of an area as C does not mean that there is necessarily a single detachment fault underlying the whole area, while identifying an area as E does not mean that there is no underlying detachment fault (see text for explanation).

4.2. Off-Axis Segmentation of the Study Area

Mapping of the off-axis segmentation was made using a number of criteria and resulted in significant differences from the segmentation map of *Gente et al.* [1995] as indicated in the introduction. Close to the spreading axis the segment boundaries must link to the nontransform offsets in the axis and must continue the morphology of the nontransform offsets on each side. Since nontransform offsets in volcanic terrain are deeper than the centers of volcanic segments, this is a primary indicator. However, in this area much of the seafloor is not volcanic, so that this simple indicator cannot be used everywhere. One important criterion mentioned above (section 3.2) is that volcanic ridges typically hook in the direction of offset close to a nontransform offset, and this allows the identification of a segment boundary where a volcanic area lies next to one formed by detachment faulting. Finally, the segment boundaries on one side of the axis should closely mirror those on the other side, taking account of the magnetic anomalies and the asymmetric spreading over much of the study area. The correspondence will not be exact, since nontransform offsets typically show an overlap parallel to the spreading axis in the ends of the volcanic ridges. Our resulting segmentation of the study area is shown in Figure 8, with the corresponding areas on each side of the spreading axis labeled.

4.3. Mapping of Tectonic Style on the Flanks of the Ridge

Figure 7 shows the distribution on the flanks of the ridge of the critical features identified above. The volcanic ridges lie mostly in separate areas from the other features. The core complexes are found as groups, and within these groups are concentrations of steep outward-facing slopes and small basins. In other areas

steep outward slopes and small basins are closely associated together, but without core complexes. The study area has been the site of major dredging and drilling programs over the years and groups of core complexes are associated with recovery of plutonic rocks. Based on these spatial associations of mapped features, we establish three terrain categories, as shown in Figure 8: Volcanic areas (V), core complex areas (C), extended terrain (E). To simplify the discussion of these areas and their relationships to one another we have divided the study area into a number of regions, based on the spreading segments at which they were generated. These are shown in Figure 7 and labeled from 1W, 1E through to 7W and 7E. We will use these abbreviations in the following text.

Volcanic areas (V) contain volcanic features clustered together, associated with clearly identifiable volcanic abyssal hill ridges. These areas contain very few steep outward slopes or oval basins. We consider that the surest way to identify type V areas is by using the small-scale bathymetric features as described above, rather than by using lithology from dredge hauls, which are abundant along the spreading axis, but uncommon on the flanks (http://www.earthchem.org/petdb). Core complex areas (C) contain groups of core complexes. The core complexes are associated with other evidence of extension (steep outward slopes and oval basins). We extend areas of type C for a short distance beyond the edges of individual core complexes since detachment faults are likely to extend below the surface beyond the exposed tops of core complexes. But we do not think that each area of C is necessarily underlain by a single detachment fault. Volcanic features are rare in such areas. Plutonic rocks have been commonly recovered from these areas where they have been sampled (see Figure 7) [*Cannat et al*., 1995b]. In the extended terrain areas (E) there are close associations of steep ($>25°$) outward slopes and oval basins, indicating significant extension by faulting, but without clear identification of exposed core complexes. Volcanic abyssal hills with shallower outward-facing slopes ($<10°$) are sometimes found in these areas, but are not common. Volcanic features dipping outward may be seen on the steep outward slopes.

The core complex areas (C) lie predominantly on the west side of the axis, independent of distance south of the Kane fracture zone and of crustal age. Extended areas (E) are more scattered, though more than 50% of the extended areas lie on the west of the axis. The central part of the map, corresponding to the region generated from Segments 2 and 3, bounded by segment boundaries north and south out to anomaly 3A, is predominantly interpreted as a volcanic area (V). There is some suggestion of an association between core complex and extended areas and the segment boundaries, and this is discussed below.

We find that core complex areas (C) make up 28% of the area overall, and 43% of the area west of the spreading center. The percentage of core complex areas is somewhat larger than the 25% estimated by *Cannat et al*. [1995b] from gravity modeling for regions of thin crust and peridotite outcrops. Extended terrain (E) makes up 16% of the area overall, and 16% of the area west of the spreading center. Volcanic areas (V) make up 56% of the area overall and 74% of the area east of the spreading center.

There is a certain degree of subjective assessment in the mapping of Figure 7. Corrugated core complexes cause no problems. Noncorrugated core complexes are more subjective, and here we have included only the three that fulfill our criteria rigorously (they are shown in Figure 5). There are other noncorrugated massifs that partially fulfill our criteria and may on further examination turn out to be core complexes, but have not been included in Figure 7. Outward slopes $>25°$ are calculated from the multibeam data, but the choice of $25°$ was arbitrary and intended to be conservative when identifying faults with significant extension [*Schouten et al*., 2010]. Small oval basins were chosen for their shape and size and interpreted to be the result of flexure associated with an extending fault, although similar basins might arise from offsets at the ends of volcanic segments. In mapping the categories of Figure 8, the association between oval basins and outward slopes $>25°$ was critical, because both of these indicate significant extension on a fault. We have not included in the core complex areas any massifs that could not be identified confidently as core complexes, and have excluded from the extended terrain several areas in which the volcanic topography has been significantly modified, but not sufficiently to generate $25°$ outward slopes and small oval basins. The result is that we have only identified significant extension where we could demonstrate it with certainty.

Ground truth for our interpretation comes from the extensive surveys that have been made in the region immediately south of the Kane fracture zone, involving geophysical investigation and extensive rock sampling that demonstrate the widespread occurrence of core complexes there [*Dick et al*., 2008]. Our interpretation is also supported by morphological comparison with characteristics recognized in other areas of the

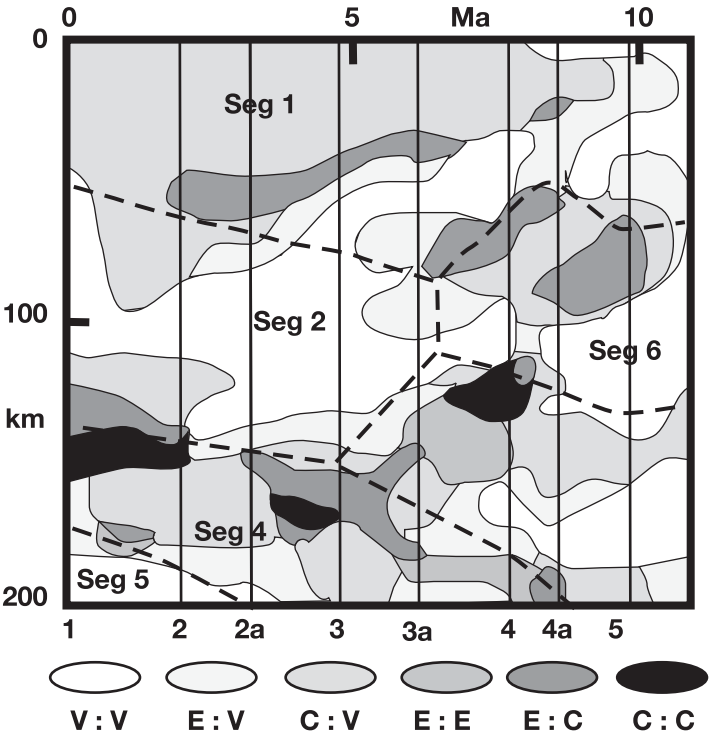

Figure 9. Evolution of the spreading axis in the area as a function of age and distance in kilometers south of the Kane fracture zone. The three types of terrain shown in Figure 8 (C, E, and V) combine to yield six different tectonically distinct types of spreading axis (C:C, C:E, E:E, C:V, E:V, and V:V). The figure was constructed from Figure 8 by combining the different types of terrain on each side of the spreading axis at each magnetic anomaly to yield a distance-crustal age map. Age is expressed by magnetic anomalies derived from Figure 1 along the bottom scale and millions of years along the top scale. Note that the pairs of corresponding anomalies are not equally distant from the spreading axis because much of the spreading was asymmetric, especially toward the north. The areas originating at the different segments are labeled and separated by dashed lines.

MAR where detailed surveys have been made in smaller areas [*Smith et al.*, 2008]. All of this information has fed into identifying the spreading mode in a given section of the study area.

4.4. Evolution of the Spreading Center Through Time

We reconstruct the nature of the spreading axis as a function of time in Figure 9. On this figure the vertical axis is distance from the Kane Fracture Zone and the horizontal axis is crustal age derived from the magnetic anomalies. The present spreading axis is along the left hand side of the figure and the magnetic anomalies are represented by vertical lines, indicating the past spreading axis at different times. By comparing the two sides of Figure 9 for a given magnetic anomaly, we can derive the nature of the axis at that time as a function of distance from the Kane Fracture zone in terms of the tectonic style on both sides of the axis. There are six different combinations of tectonic style and these are plotted in Figure 9. In V:V, volcanic crust faces volcanic crust on each side of the axis, E:V covers areas where extended crust faces volcanic crust, C:V covers areas where core complex crust faces volcanic crust, E:E covers areas in which extended terrain lies on both sides of the axis, C:E covers areas where core complex crust faces extended crust, and C:C covers areas where core complex crust lies on both sides of the axis. As an example, at anomaly 2A time, the first 45 km of the axis, starting at the Kane Fracture Zone was C:V, with core complex facing volcanic across the axis. The next 16 km was C:E, with core complex facing extended terrain across the axis, and so on. The six different types of spreading mode in Figure 9 cover the following areas: V:V 28%, E:V 17%, C:V 36%, E:E 3%, C:E 12%, and C:C 4%.

Because of the uncertainty about the precise position of the magnetic anomalies and the subjective nature of our interpretation in Figure 8 (see above), these maps have the potential for some adjustment. We experimented with possible alternative positions for the anomalies and with three different versions of Figure 8, but those adjustments did not affect the overall shapes of the plotted areas in Figure 9 significantly.

5. Discussion

5.1. Patterns in the Spreading Mode Through Time

On the west side of Figure 8 there are two regions of core complexes at the north and south edges of the map. These have increasingly extended away from the limiting fracture zones since they were initiated at anomaly 5 time (about 10 Ma) and are still active now. The northern region of core complexes started in area 1W and propagated southward steadily to form a triangular shape. This triangle extended into area 2W at anomaly 2A time with no apparent deviation of its southern border. The south region grew similarly,

occupying most of area 4W until anomaly 2A time (about 3 Ma) when the volcanic Segment 5 penetrated through the southern transform fault and entered the study area. Two other groups of core complexes were present in the center of the study region on the west flank already by anomaly 5 time, one of them in 6W and the other in 7W, with a gap in it. These died away shortly after anomaly 4 time (about 8 Ma), as the core complex areas north and south grew wider. The areas of extended terrain on the west are borders to core complex areas.

On the east side of the axis, two areas of core complexes were initiated in the southern part of the area, one after the other. The first, in 4E and adjacent areas, ran from anomaly 4A to anomaly 2A time and the second in 2E from anomaly 2 time to the present. Farther north in 6E and 1E a group of three sections of extended terrain lasted from anomaly 5 to anomaly 3 time.

In many other locations, core complexes have been linked to the presence of transform or nontransform offsets of the spreading axis. Are there any similar links in our study area? The broad triangular region in 1W originated at the Kane transform at an inside corner and grew southward from there while remaining attached to the transform. Similarly, the region at the south side of the west flank in 7W and 4W also originated at a ridge-transform inside corner and extended northward, but its present-day area is not related to any transform offset. The north side of the same region closely follows the northern boundary of Segment 4 and the borders of several other core complex areas follow other segment boundaries closely such as those that lie close to the boundary between 2E and 4E. The evolution through time of the broad triangular core complex area to the north is an exception to this relationship. This area grew southward as it evolved and extended directly across the border between Segment 1 and Segment 2 to occupy eventually nearly the whole of the length of Segments 1 and 2 at the spreading axis.

Are the detachment faults that cap the core complexes linked together at depth into a single continuous fault? Does such a fault rise to expose the fault surface at the top of corrugated complexes and then fall below the level of the ocean floor at their sides? Or is each core complex the exposure of a different detachment fault? In parts of the large C area just south of Kane transform individual corrugations can be traced from one core complex to the next, indicating that close to the transform valley the core complexes are linked to a single fault extending in the spreading direction. The faults that cap other groups of core complexes may similarly be linked at depth in the spreading direction. But there are exceptions. *Dick et al*. [2008] concluded that there was a short break between two episodes of detachment faulting during the evolution of the Kane Megamullion. A model in which a single detachment fault continues along axis from segment end to center has been proposed in other areas based on seismic data [*Reston and Ranero*, 2011], and there is evidence from continental detachments for linking of detachment domes perpendicular to the extension direction [*McCarthy et al*., 1991; *Wong and Gans*, 2008]. The areas of E are of course more problematic, especially since there is no certainty that they are related to a buried detachment fault or to incipient detachment faults. In areas of E that are linked to areas of C the chance must be greater that the faults sole out into an underlying single detachment. These questions about the possible interlinking of core complex domes and extended terrain may well be answered by further research, especially into local seismicity or by using seismic reflection profiling.

5.2. Evolution of the Spreading Axis Through Time

The spacing of the magnetic anomalies in Figures 1 and 8 clearly demonstrates the asymmetric spreading toward the north end of the study area. At the north, the west side has spread about 1.4 times faster than the east side since anomaly 5. This asymmetry persists as far south as the Segment 3–4 boundary. South of that, the spreading has been more nearly symmetrical. It is an interesting question whether the presence of a major area of core complexes in the north is a result of the asymmetry or has been a cause of it. The asymmetric spreading will have resulted in eastward migration of the spreading axis in the north relative to the axis in the south.

Figure 9 shows variation in the modes of spreading at the axis through time. Before anomaly 5 the spreading axis was V:V over most of the study area. Since then, the north and south parts of the study area have followed two very different evolutionary histories of the spreading axis. In the south, patches of C:C and E:C are linked by a strip of C:V that follows in a general way the pattern of segment boundaries in this part of the study area. In the north there has been a long-standing spreading mode (C:V) where core complexes form on the west and volcanism on the east. This spreading mode has grown southward through time.

Since Anomaly 5 there has in general been 20–30 km of C:C, E:E or C:E spreading along the 200 km of spreading axis at any one time (i.e., 10–13% of the total length of ridge axis), with C:C and E:E being relatively less extensive than C:E. V:V has typically accounted for about 50 km of the axis at any one time (~25% of the ridge axis length). The rest of the ridge axis (typically about 120 km or 60%) has been C:V or E:V.

5.3. Transition From One Spreading Mode to Another

Is the transition from one spreading mode to another abrupt or gradual? How is it related to segment boundaries? Figure 8 shows that the edges of many of the core complex C areas and some of the E areas are close to segment boundaries. Across a segment boundary, the transition to V is typically abrupt, indicating a rapid change in the conditions that control the mode of spreading from one segment to the next. Transitions within segments seem more gradual, with C areas commonly mantled by E areas and then by V. But several transitions are more abrupt than this, so that the noncorrugated core complex at 22°30′N, 45°W seems to have arisen abruptly within a V segment.

The large C area close to Kane shows a transition at a larger scale. The southern edge of this has propagated southward over 10 Ma, beginning by extending 25 km south of the Kane transform and then growing southward to reach 100 km south of Kane by the present. In doing so it has gradually replaced the V area in the west side of Segment 1, and eventually has crossed the boundary between 1W and 2W, expanding at the expense of the volcanic area on the west side of Segment 2. As the transition crossed the segment boundary, the propagating C area became mantled by a narrow E area that was generated within Segment 2. These observations on the transitions between modes suggest that whatever conditions act to stabilize one spreading mode rather than another cannot be simply defined at present.

5.4. Magmatism and Mode of Spreading

An important strand in discussion of long-lived faults and core complex formation is the relation between detachment faulting and magmatism. Numerical models of spreading generate detachment faults as the fraction of spreading by magmatism (*M*) decreases [*Buck et al*., 2005; *Olive et al*., 2010; *Tucholke et al*., 2008]. Similarly, core complexes are commonly found close to transform faults where magmatism is expected to be weak because of cooling through the transform fault plane. Inside corner positions seem to be favored [e.g., *Blackman et al*., 2002; *Tucholke and Lin*, 1994; *Tucholke et al*., 1998] perhaps because of the advection of cool lithosphere past the newly formed crust, while in outside corners the two plates are welded together. The same conditions exist to a lesser extent at segment boundaries marked by small, nontransform offsets.

The relation between crustal thickness determined by gravity and magma supply has been widely accepted [*Maia and Gente*, 1998; *Wang et al*., 2015; *Gente et al*., 1995] Evolution and segmentation characteristics of a slowly spreading mid-ocean ridge, submitted, 1993], but is open to question as Maia and Gente pointed out. It assumes that the crust is entirely magmatic, which the work in the study area early demonstrated is incorrect [*Cannat et al*., 1995b] and that an overall density of 2.75 Mg/m^3 can be applied to magmatic rocks, despite the significant difference in density between volcanics and gabbro. A section rich in serpentinite will seem to be thicker and more volcanic than it is, while a large magmatic proportion of gabbro will seem to be thinner crust than it is. Thus only a broad correlation can be expected between crustal thickness determined by gravity and the actual supply of magma. Figure 10 shows that there is an overall, though moderate, relationship between the gravity anomalies in *Maia and Gente* [1998] and the pattern of spreading modes in Figure 9 that indicates that at a general level both indicators are responding to similar geological conditions.

The large areas of C at the north and south edges of the study area (in 1W and 2W, 7W and 4W) originated at inside corners of the two transform faults at around anomaly 5 time. The other areas of C and E in the south of the study area are associated in a general way with segment boundaries. These areas are also associated with low gravity anomalies [*Cannat et al*., 1995b]. But the inside corner model does not explain the steady growth of the areas of C away from the transforms at both the north and south ends of the study area since anomaly 5 time. Does that growth mean that the supply of magma to the spreading centers in the study area has decreased with time? That would imply that the ridge axis was especially magmatically active 7–10 Ma ago, and that magma supply has decreased steadily since then. But that does not appear to

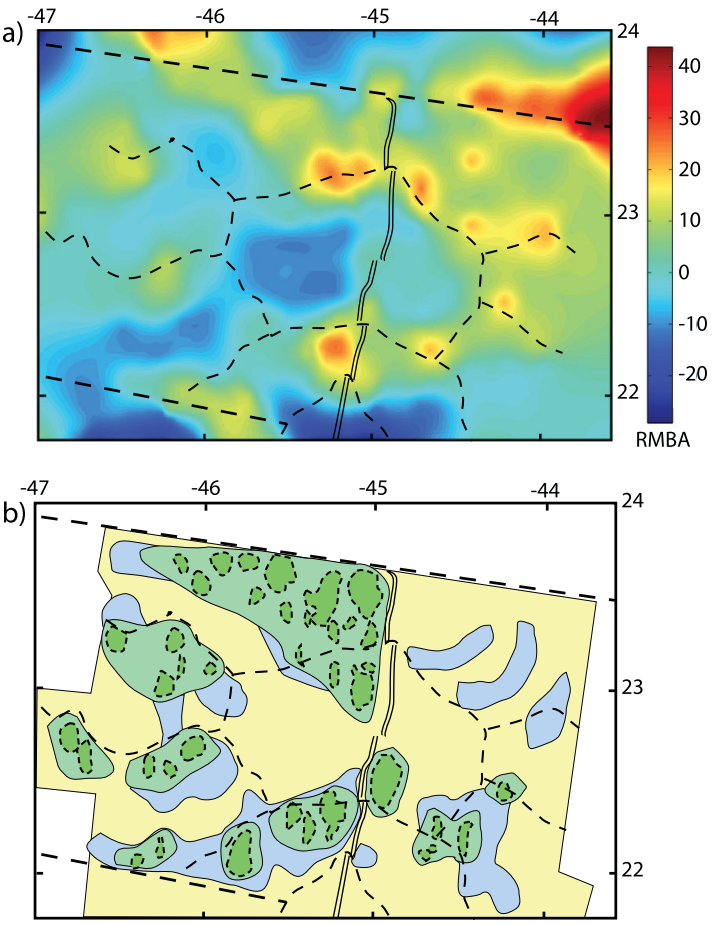

Figure 10. Comparison of a simplified version of Figure 8 with RMBA anomalies digitized from *Maia and Gente* [1998]. Higher RMBA values are associated with denser underlying rocks and hence, by association, with thinner crust, while lower residual gravity anomalies are associated with lower density underlying rocks, and hence with thinner crust. There is a general relationship between the two images, but not a precise one. See text for discussion.

be the case, since at those early times substantial areas of core complexes occur at the center of the west part of the study area in 6W and 7W, so that the total length of C+E on the west side of the axis at anomaly 4A time was the same as it is today (Figure 8) implying an overall magma supply then close to that of today.

As the large region of C in the north of the study area expanded southward, it crossed the boundary between 1W and 2W at anomaly 2A time. On the magmatic model this would imply that the magma supply to Segment 2 had decreased. Yet the northern boundary of Segment 2 has been propagating northward steadily since anomaly 4 time (Figure 8), suggesting that Segment 2 has for long time been magmatically more active than Segment 1. The Segments 1–2 boundary is especially well developed on the east side of the axis (Figure 1). Though Segment 1 has for a long time had a C:V axis, it is not a magmatically weak segment, since it has in the past 10 Ma regularly sent a major volcanic ridge into the nodal basin, as seen in the fracture zone on the east side of the axis (Figures 1 and 3c). These episodes of enhanced magmatism do not seem to have been reflected in changes in the core complex activity on the west side of the axis. The present axis of Segment 1, in the median valley just south of the Kane fracture zone, is marked by a large, young axial volcanic ridge that hosts the Snake Pit black smoker field [*Brown and Karson*, 1988; *Karson et al*., 1987] and is underlain by a hot and/or melt-rich lower crust [*Canales et al*., 2000]. It extends all the way into the transform valley. Morphologically it does not appear to be magmatically weak now, yet is bordered by a line of core complexes on its west side.

It has been argued that for detachment faulting to start, the magma supply at the axis must be weak [e.g., *Tucholke et al*., 1998], implying that $M < 0.5$. According to the numerical modeling of *Tucholke et al*. [2008], detachment faulting occurs when $0.5 > M > 0.3$. Along the present spreading axis, where the axis type is V:V or C:V there is always clear morphological evidence for current (or at least very recent) volcanism. In the 30 km of the current spreading axis close to the boundary between Segments 3 and 4, that is C:E or C:C the morphological evidence for active volcanism is weaker. The axial volcanic ridges in those sections of the axis are smaller than those to the north and south. If we follow the results of the numerical modeling, (that detachment faulting implies $0.3 < M < 0.5$) this might imply that the presence of a large axial volcanic ridge in a C:V segment indicates that M is close to 0.5 and when the axial volcanic ridge is smaller, M is less than this but still >0.3. Coupled with the modeling results, the complex patterns of spreading mode in the study area suggest that over large parts of the area the magma supply is close to the threshold between

different modes of spreading. This implies that small variations in magma supply may cause a switch from one mode to the other. It also suggests that other factors than magma supply, such as the local tectonic history, may exert an influence to tip the mode from one type to another. This is supported by the apparent discrepancies between simple local magma supply and mode of spreading that were described above.

5.5. Feedback Stabilizing Detachment Faulting

In parallel with the effect of magma supply, it is possible that once a core complex has formed in an inside corner then there is a positive feedback that allows core complexes to extend and develop farther and farther from the transforms. This might account for the widening of the northern area of core complexes from about 20 km 7–10 Ma ago to 100 km in recent times. Certainly it is hard to account for the 100 km of width of the core complex area at the north to processes currently acting at the inside corner there. And such a feedback may account for the gradual continuing increase in width of the core complex area at the south of the area even though the inside corner there was removed when volcanic Segment 5 propagated across it 3 Ma ago.

What might drive such a feedback? There are two basically competing processes during ocean floor spreading during core complex formation. One is intrusion of magma in dikes and the other is slip on detachment faults. Intrusion of dikes is controlled by the internal pressure in the magma chamber and the least compressive stress $\sigma 3$ in the wall rocks [*Buck*, 2006]. Of these the magma chamber pressure is related to overall magma recharge and $\sigma 3$ to the extensional strain since the last spreading event. Slip events on the detachment faults are related also to $\sigma 3$, but also to the frictional resistance to slip on the fault plane. In detachment faults the material in the fault may originally have been crushed basalt, but in detachment faults the fault rock has commonly been transformed to serpentinite [*Andreani et al*., 2007; *Boschi et al*., 2006] or (if gabbro is close by) to talc [*McCaig et al*., 2007]. These materials have a much lower frictional resistance than crushed rock, meaning that slip will take place on such a fault at much lower $\sigma 3$. Under these conditions fault slip will be favored over dyke intrusion until magma chamber pressure has built to a high level.

This effect would allow the feedback that we seek. In a spreading environment in which a V:V segment lies adjacent to a C:V segment, the presence of a freely slipping serpentinite-rich fault next to a fault filled with more resistive crushed rock would lead to the serpentinite-rich fault propagating laterally to take over the extension in the V:V segment, inhibiting the intrusion of dikes. The gradients on the southern side of the C area in segment 1W and on the northern side of 4W and 7W, the two large and apparently anomalous areas of detachment faulting in the study area are similar, about 10 km per million years to the south and to the north, or about 10 mm/a, comparable with the half-spreading rate.

The mechanical properties of the different rocks involved may thus be important in defining the response of the lithosphere to extension, as suggested in another context by *Cannat et al*. [2009].

6. Conclusions

Bathymetric morphology is an important element in determining tectonic interpretations at the MAR. Using three categories of bathymetric information it is possible to map differing degrees of extension by faulting: volcanic, with minor faulting, extended volcanic, where volcanic features have been rotated significantly during extension, and core complex, where extension by long-lived detachment faulting is dominant. The mapping shows that the generally detachment-rich character of the South of Kane study area continues throughout the 10 Ma period since anomaly 5. There is a major asymmetry in detachment faulting between the west and east sides of the axis in the northern half of the study area and a possible correlation between asymmetry of spreading and of detachments, with the faster-spreading western side more detachment-rich. As the median valley has evolved there have been rapid transitions between detachment faulting and volcanic construction.

In the southern part of the area, detachment faulting is linked in a general way to segment boundaries and to the inside corner of an extinct fracture zone. This pattern of faulting is very likely related to lower magma supply at segment ends. For short periods of time in this area two detachment faults have faced one another across the spreading axis, indicating spreading with markedly less than 50% magmatic spreading.

On the west side of the northern part of the study area a major triangular region of core complex formation was initiated at the inside corner of the Kane fracture zone at anomaly 5 time and resulted in a string of at

least six core complexes close to the fracture zone up to the present time. At the same time the triangle of core complexes grew broader toward the south, reaching a breadth of 100 km and eventually breaching a major segment boundary. The initiation of this triangle was probably related directly to magma supply. But its continued growth suggests the operation of an additional mechanism, a competition between dyke intrusion and detachment fault slip that is won by detachment faulting where the fault plane has become filled with materials such as serpentinite or talc with their low frictional resistance to slip.

Acknowledgments

The multibeam bathymetry data in this paper are publicly available from the Global Multiresolution Topography Data Portal (http://www.marine-geo.org/portals/gmrt/). The bathymetry data were displayed using the Generic Mapping Tools (GMT) software [*Wessel and Smith*, 1991]. We are grateful to Mathilde Cannat and Pascal Gente for arranging for the release of the bathymetry data to the Global Multiresolution Data Portal. D.K.S. was supported in part by Woods Hole Oceanographic Institution. We had many helpful discussions with other scientists working on the Mid-Atlantic Ridge, and especially with Brian Tucholke, Mathilde Cannat, Tim Reston, and Andrew McCaig. We thank our two anonymous referees for their helpful comments and criticisms. This is IPGP contribution 3639.

References

Andreani, M., C. Mével, A. M. Boullier, and J. Escartín (2007), Dynamic control on serpentine crystallization in veins: Constraints on hydration processes in oceanic peridotites, *Geochem. Geophys. Geosyst.*, *8*, Q02012, doi:10.1029/2006GC001373.

Ballard, R. D., and T. H. van Andel (1977), Morphology and tectonics of the inner rift valley at lat 36°50′N on the Mid-Atlantic Ridge, *Geol. Soc. Am. Bull.*, *88*, 507–530.

Becker, K., M. G. Langseth, and R. D. Hyndman (1984), Temperature measurements in Hole 395A, Leg 78B, in *Initial Reports-Deep Sea Drilling Project*, vol. 78B, edited by R. D. Hyndman et al., pp. 689–698, U.S. Gov. Print. Off., Washington, D. C., doi:610.2973/dsdp.proc.2978b.2105.1984.

Blackman, D. K., et al. (2002), Geology of the Atlantis Massif (Mid-Atlantic Ridge, 30°N): Implications for the evolution of an ultramafic oceanic core complex, *Mar. Geophys. Res.*, *23*, 443–469.

Boschi, C., G. L. Früh-Green, A. Delacour, J. A. Karson, and D. S. Kelley (2006), Mass transfer and fluid flow during detachment faulting and development of an oceanic core complex, Atlantis Massif (MAR 30°N), *Geochem. Geophys. Geosyst.*, *7*, Q01004, doi:10.1029/2005GC001074.

Brown, J., and J. A. Karson (1988), Variations in axial processes on the Mid-Atlantic Ridge: The median valley of the MARK area, *Mar. Geophys. Res.*, *10*(1), 109–138.

Bryan, W. B., G. Thompson, and J. N. Ludden (1981), Compositional variation in normal MORB from 22°-25° N: Mid-Atlantic Ridge and Kane Fracture Zone, *J. Geophys. Res.*, *86*, 11,815–811,836.

Buck, W. R. (1988), Flexural rotation of normal faults, *Tectonics*, *7*, 959–973.

Buck, W. R. (Ed.) (2006), *The Role of Magma in the Development of the Afro-Arabian Rift System*, Geol. Soc., London, U. K.

Buck, W. R., L. L. Lavier, and A. N. B. Poliakov (2005), Modes of faulting at mid-ocean ridges, *Nature*, *434*, 719–723.

Canales, J. P., J. A. Collins, J. Escartin, and R. S. Detrick (2000), Seismic structure across the rift valley of the Mid-Atlantic ridge at 23°20′N (MARK area): Implications for crustal accretion processes at slow-spreading ridges, *J. Geophys. Res.*, *105*, 28,411–28,425.

Cannat, M., et al. (1995a), *Proceedings of the Ocean Drilling Program, Initial Reports*, 798 pp., Ocean Drill. Program, College Station, Tex.

Cannat, M., et al. (1995b), Thin crust, ultramafic exposures, and rugged faulting patterns at the Mid-Atlantic Ridge (22°-24°N), *Geology*, *23*, 49–52.

Cannat, M., D. Sauter, V. Mendel, E. Ruellan, K. Okino, J. Escartin, V. Combier, and M. Baala (2006), Modes of seafloor generation at a melt-poor ultraslow-spreading ridge, *Geology*, *34*(7), 605–608.

Cannat, M., D. Sauter, J. Escartín, L. L. Lavier, and S. Picazo (2009), Oceanic corrugated surfaces and the strength of the axial lithosphere at slow spreading ridges, *Earth Planet. Sci. Lett.*, *288*(1–2), 174–183.

Dannowski, A., I. Grevemeyer, C. R. Ranero, G. Ceuleneer, M. Maia, J. P. Morgan, and P. Gente (2010), Seismic structure of an oceanic core complex at the Mid-Atlantic Ridge, 22°19′N, *J. Geophys. Res.*, *115*, B07106, doi:10.1029/2009JB006943.

deMartin, B. J., R. A. Reves-Sohn, J. P. Canales, and S. E. Humphris (2007), Kinematics and geometry of active detachment faulting beneath the TAG hydrothermal field on the Mid-Atlantic Ridge, *Geology*, *35*(8), 711–714.

Detrick, R. S., et al. (1990), *Proceedings of Ocean Drilling Program, Scientific Results*, vol. 106/109, Ocean Drill. Program, College Station, Tex.

Dick, H. J. B., M. A. Tivey, and B. E. Tucholke (2008), Plutonic foundation of a slow-spreading ridge segment: Oceanic core complex at Kane Megamullion, 23°30′N, 45°20′W, *Geochem. Geophys. Geosyst.*, *9*, Q05014, doi:10.1029/2007GC001645.

Durand, C., V. Ballu, P. Gente, and J. Dubois (1996), Horst and graben structures on the flanks of the Mid-Atlantic Ridge in the MARK area (23°22′N): Submersible observations, *Tectonophysics*, *265*, 275–297.

Edwards, K. J., W. Bach, A. Klaus, and the Expedition 336 Scientists (2012), Expedition 336 Summary, *Proceedings of the Integrated Ocean Drilling Program, 336*, Integrated Ocean Drilling Program Management International, Inc., Tokyo, doi:10.2204/iodp.proc.336.101.2012.

Escartín, J., D. K. Smith, J. Cann, H. Schouten, C. H. Langmuir, and S. Escrig (2008), Central role of detachment faults in accretion of slow-spread oceanic lithosphere, *Nature*, *455*, 790–794, doi:10.1038/nature07333.

Garces, M., and J. S. Gee (2007), Paleomagnetic evidence of large footwal rotations associated with low-angle faults at the Mid-Atlantic Ridge, *Geology*, *35*, 279–282.

Gente, P., R. A. Pockalny, C. Durand, C. Deplus, M. Maia, G. Ceuleneer, C. Mevel, M. Cannat, and C. Laverne (1995), Characteristics and evolution of the segmentation of the Mid-Atlantic Reidge between 20°N and 24°N during the last 10 million years, *Earth Planet. Sci. Lett.*, *129*, 55–71.

Gillis, K., and G. Thompson (1993), Metabasalts from the Mid-Atlantic Ridge: New insights into hydrothermal systems in slow-spreading crust, *Contrib. Mineral. Petrol.*, *113*, 502–523.

Grevemeyer, I., T. J. Reston, and S. Moeller (2013), Microseismicity of the Mid-Atlantic Ridge at 7°S–8°15′S and at the Logatchev Massif oceanic core complex at 14°40′N–14°50′N, *Geochem. Geophys. Geosyst.*, *14*, 3532–3554, doi:10.1002/ggge.20197.

Karson, J. A. (1999), Geological investigation of a lineated massif at the Kane Transform Fault: Implications for oceanic core complexes, *Philos. Trans. R. Soc. London A*, *357*, 713–740.

Karson, J. A., and J. R. Brown (1988), Geologic setting of the Snake Pit hydrothermal site: An active vent field on the Mid-Atlantic Ridge, *Mar. Geophys. Res.*, *10*, 91–107.

Karson, J. A., and H. J. B. Dick (1983), Tectonics of ridge-transform intersections at the Kane fracture zone, *Mar. Geophys. Res.*, *6*, 51–98.

Karson, J. A., et al. (1987), Along-axis variations in seafloor spreading in the MARK area, *Nature*, *328*, 681–685.

Kong, L. S., R. S. Detrick, P. J. Fox, L. A. Mayer, and W. B. F. Bryan (1988), The morphology and tectonics of the MARK area from sea beam and sea MARC I observations (Mid-Atlantic Ridge 23°N), *Mar. Geophys. Res.*, *10*, 59–90.

MacLeod, C. J., et al. (2002), Direct geological evidence for oceanic detachment fauling: The Mid-Atlantic Ridge, 15°45′N, *Geology*, *30*(10), 279–282.

MacLeod, C. J., R. C. Searle, B. J. Murton, J. F. Casey, C. Mallows, S. C. Unsworth, K. L. Achenbach, and M. Harris (2009), Life cycle of oceanic core complexes, *Earth Planet Sci. Lett.*, *287*, 333–344.

MacLeod, C. J., J. Calut, J. Escartin, H. Horen, and A. Morris (2011), Quantitative constraint on footwall rotations at the 15°45′N oceanic core complex, Mid-Atlantic Ridge: Implications for oceanic detachment fault processes, *Geochem. Geophys. Geosyst.*, *12*, Q0AG03, doi: 10.1029/2011GC003503.

Maia, M., and P. Gente (1998), Three-dimensional gravity and bathymetry analysis of the Mid-Atlantic Ridge between 20°N and 24°N: Flow geometry and temporal evolution of the segmentation, *J. Geophys. Res.*, *103*, 951–974.

Mallows, C., and R. C. Searle (2012), A geophysical study of oceanic core complexes and surrounding terrain, Mid-Atlantic Ridge 13°N–14°N, *Geochem. Geophys. Geosyst.*, *13*, Q0AG08, doi:10.1029/2012GC004075.

McCaig, A., B. Cliff, J. Escartín, A. E. Fallick, and C. MacLeod (2007), Oceanic detachment faults focus very large volumes of black smoker fluids, *Geology*, *35*, 935–938, doi:10.1130/G23657A.1.

McCarthy, J., S. P. Larkin, G. S. Fuis, R. W. Simpson, and K. A. Howard (1991), Anatomy of a metamorphic core complex: Seismic refraction/wide-angle reflection profiling in southeastern California and western Arizona, *J. Geophys. Res.*, *96*, 12,259–12,291.

Melson, W. G., G. Thompson, and T. H. v. Andel (1968), Volcanism and metamorphism in the Mid-Atlantic Ridge, 22°N latitude, *J. Geophys. Res.*, *73*, 5925–5941.

Melson, W. G., P. D. Rabinowitz, H. Bougault, T. Fuji, A. L. Graham, H. P. Johnson, J. H. Natland, E. C. Prosser, J. M. Rhodes, and B. P. Zolotarev (Eds.) (1979), *Initial Reports of the Deep Sea Drilling Project Leg 45*, Ocean Drill. Program, College Station, Tex.

Miyashiro, A., F. Shido, and M. Ewing (1971), Metamorphism in the Mid-Atlantic Ridge near 24° and 30°N, *Philos. Trans. R. Soc. London A*, *268*, 589–603.

Morris, A., J. S. Gee, N. Pressling, B. E. John, C. J. MacLeod, C. B. Grimes, and R. C. Searle (2009), Footwall rotation in an oceanic core complex quantified using reoriented integrated ocean drilling program core samples, *Earth Planet. Sci. Lett.*, *287*(1–2), 217–228.

Ohara, Y., T. Yoshida, and S. Kasuga (2001), Giant megamullion in the Perece Vela Backarc basin, *Mar. Geophys. Res.*, *22*, 47–61.

Okino, K., K. Matsuda, D. Christie, Y. Nogi, and K. Koizumi (2004), Development of oceanic detachment and asymmetric spreading at the Australian-Antarctic Discordance, *Geochem. Geophys. Geosyst.*, *5*, Q12012, doi:10.1029/2004GC000793.

Olive, J.-A., M. D. Behn, and B. E. Tucholke (2010), The structure of oceanic core complexes controlled by the depth distribution of magma emplacement, *Nat. Geosci.*, *3*, 491–495, doi:10.1038/NGEO1888.

Pockalny, R. A., R. Detrick, and P. J. Fox (1988), Morphology and tectonics of the Kane transform from Sea Beam bathymetry data, *J. Geophys. Res.*, *93*, 3179–3193.

Pockalny, R. A., A. Smith, and P. Gente (1995), Spatial and temporal variability of crustal magnetization of a slowly spreading ridge: Mid-Atlantic Ridge (20°-24°N), *Mar. Geophys. Res.*, *17*, 301–320.

Purdy, G. M., and R. S. Detrick (1986), Crustal structure of the Mid-Atlantic Ridge at 23°N from seismic refraction studies, *J. Geophys. Res.*, *91*, 3739–3762.

Reston, T. J., and C. R. Ranero (2011), The 3-D geometry of detachment faulting at mid-ocean ridges, *Geochem. Geophys. Geosyst.*, *12*, Q0AG05, doi:10.1029/2011GC003666.

Sauter, D., et al. (2013), Continuous exhumation of mantle-derived rocks at the Southwest Indian Ridge for 11 million years, *Nat. Geosci.*, *6*, 314–320, doi:10.1038/ngeo1771.

Schouten, H., D. K. Smith, J. R. Cann, and J. Escartin (2010), Tectonic versus magmatic extension in the presence of core complexes at slow-spreading ridges from a visualization of faulted seafloor topography, *Geology*, *38*, 615–618, doi:10.1130/G30803.30801.

Schroeder, T. J., M. Cheadle, H. J. B. Dick, U. Faul, J. F. Casey, and P. B. Kelemen (2007), Non-volcanic seafloor spreading and corner-flow rotation accommodated by extensional faulting at 15°N on the Mid Atlantic Ridge: A structural synthesis of ODP Leg 209, *Geochem. Geophys. Geosyst.*, *8*, Q06015, doi:10.1029/2006GC001567.

Searle, R. C., et al. (2010), Structure and development of an axial volcanic ridge: Mid-Atlantic Ridge, 45°N, *Earth Planet. Sci. Lett.*, *299*(1–2), 228–241.

Sempéré, J. C., J. Lin, H. S. Brown, H. Schouten, and G. M. Purdy (1993), Segmentation and morphotectonic variations along a slow-spreading center: The Mid-Atlantic Ridge (24°N-30°40′N), *Mar. Geophys. Res.*, *15*, 153–200.

Shaw, P. R., and J. Lin (1993), Causes and consequences of variations in faulting style at the Mid-Atlantic Ridge, *J. Geophys. Res.*, *98*, 21,839–21,851.

Smith, D. K., and J. R. Cann (1999), Constructing the upper crust of the Mid-Atlantic Ridge: A reinterpretation based on the Puna Ridge, Kilauea Volcano, *J. Geophys. Res.*, *104*, 25,379–25,399.

Smith, D. K., J. Escartin, M. Cannat, M. Tolstoy, C. G. Fox, D. Bohnenstiehl, and S. Bazin (2003), Spatial and temporal distribution of seismicity along the northern Mid-Atlantic Ridge (15°-35°N), *J. Geophys. Res.*, *108*(B3), 2167, doi:10.1029/2002JB001964.

Smith, D. K., J. R. Cann, and J. Escartin (2006), Widespread active detachment faulting and core complex formation near 13°N on the Mid-Atlantic Ridge, *Nature*, *442*, 440–443. doi:10.1038/nature04950.

Smith, D. K., J. Escartin, H. Schouten, and J. R. Cann (2008), Fault rotation and core complex formation: Significant processes in seafloor formation at slow-spreading mid-ocean ridges (Mid-Atlantic Ridge, 13–25°N), *Geochem. Geophys. Geosyst.*, *9*, Q03003, doi:10.1029/2007GC001699.

Smith, D. K., et al. (2014), Development and evolution of detachment faulting along 50 km of the Mid-Atlantic Ridge near 16.5°N, *Geochem. Geophys. Geosys.*, *15*, 4692–4711, doi:10.1002/2014GC005563.

Thibaud, R., P. Gente, and M. Maia (1998), A systematic analysis of the Mid-Atlantic Ridge morphology and gravity between 15°N and 40°N: Constraints of the thermal structure, *J. Geophys. Res.*, *103*, 24,223–24,243.

Toomey, D. R., S. C. Solomon, and G. M. Purdy (1988), Microearthquakes beneath the median valley of the Mid-Atlantic Ridge near 23°N: Tomography and tectonics, *J. Geophys. Res.*, *93*, 9093–9112.

Tucholke, B. E., and J. Lin (1994), A geological model for the structure of ridge segments in slow spreading ocean crust, *J. Geophys. Res.*, *99*, 11,937–911,958.

Tucholke, B. E., J. Lin, and M. C. Kleinrock (1998), Megamullions and mullion structure defining oceanic metamorphic core complexes on the mid-Atlantic ridge, *J. Geophys. Res.*, *103*, 9857–9866.

Tucholke, B. E., M. D. Behn, W. R. Buck, and J. Lin (2008), Role of melt supply in oceanic detachment faulting and formation of megamullions, *Geology*, *36*, 455–458, doi:10.1130/G24639A.24631.

Wang, T., B. E. Tucholke, and J. Lin (2015), Spatial and temporal variations in crustal production at the Mid-Atlantic Ridge, 25°N-27°30′N and 0–27 Ma, *J. Geophys. Res. Solid Earth*, *120*, 2119–2142, – doi:10.1002/2014JB011501.

Wessel, P., and W. H. F. Smith (1991), Free software helps map and display data, *Eos Trans. AGU*, *72*, 441–446.

Williams, C. M. (2007), Oceanic lithosphere magnetization: Marine magnetic investigations of crustal accretion and tectonic processes in mid-ocean ridge environments, PhD thesis, 285 pp., MIT Press, Woods Hole.

Wong, M. S., and P. B. Gans (2008), Geologic, structural, and thermochronologic constraints on the tectonic evolution of the Sierra Mazatán core complex, Sonora, Mexico: New insights into metamorphic core complex formation, *Tectonics*, *27*, TC4013, doi:10.1029/2007TC002173.